Journal of Asian Ceramic Societies

ISSN: (Print) (Online) Journal homepage: https://www.tandfonline.com/loi/tace20

Pulsed electrodeposition of Ni-B/TiN composites: effect of current density on the structure, mechanical, tribological, and corrosion properties

Fatih Doğan , Mehmet Uysal , Erhan Duru , Hatem Akbulut & Serdar Aslan

To cite this article: Fatih Doğan , Mehmet Uysal , Erhan Duru , Hatem Akbulut & Serdar Aslan (2020) Pulsed electrodeposition of Ni-B/TiN composites: effect of current density on the structure, mechanical, tribological, and corrosion properties, Journal of Asian Ceramic Societies, 8:4, 1271-1284, DOI: 10.1080/21870764.2020.1840704

To link to this article: https://doi.org/10.1080/21870764.2020.1840704

Published online: 14 Nov 2020.

JOURNAL OF ASIAN CERAMIC SOCIETIES
2020, VOL. 8, NO. 4, 1271–1284
https://doi.org/10.1080/21870764.2020.1840704

THE CERAMIC SOCIETY OF JAPAN
THE KOREAN CERAMIC SOCIETY
Taylor & Francis
Taylor & Francis Group

FULL LENGTH ARTICLE

Pulsed electrodeposition of Ni-B/TiN composites: effect of current density on the structure, mechanical, tribological, and corrosion properties

Fatih Doğan [a], Mehmet Uysal [b], Erhan Duru [b], Hatem Akbulut [b,c,d] and Serdar Aslan [b]

[a]Institute of Natural Sciences, Metallurgy and Materials Engineering, Sakarya University, Sakarya, Turkey; [b]Faculty of Engineering, Department of Metallurgy and Materials Engineering, Sakarya University, Sakarya, Turkey; [c]Central Research Laboratory (SARGEM), Esentepe Campus, Sakarya, Turkey; [d]Technology Development Zones, NESSTEC Energy & Surface Technologies A.S., Sakarya, Turkey

ABSTRACT

Ni-B/TiN composite coatings with different current densities (1.5, 3.0, 4.5, and 6.0 A/dm^2) have been successfully produced on a mild steel substrate using the pulsed electrodeposition (PED) method. The effect of current density on structure, morphology, hardness, tribological, and corrosion behaviors were investigated. It was found that the composite coating produced with a current density of 4.5 A/dm^2 exhibited, smooth surface a uniform fine compact and crack-free structure and the particles were distributed homogeneously in the metallic matrix. After the Ni-B/TiN composite coatings deposited on the substrate, samples were heat treated at 400 C for 1 h for providing precipitation of intermetallics to improve mechanical and tribological properties. In the electrochemical measurements performed in 3.5% NaCl solution by weight, the anticorrosion ability of the composite coating was analyzed. According to the results obtained that current density is an important parameter affecting not only the deposition mechanism of Ni-B/TiN composite depositions but also microstructural, mechanical, tribological, and corrosion properties in the PED process. Accordingly, TiN particle reinforced Ni-B composite coatings deposited by the PED method are expected to be applied as a protective coating in industrial applications with excellent hardness, superior wear resistance and anticorrosion capability.

ARTICLE HISTORY
Received 11 August 2020
Accepted 19 October 2020

KEYWORDS
Pulse-co-deposition; current densiy; Ni-B/TiN composite; wear and friction; corrosion resistance; Gugliemi's model

1. Introduction

On an industrial scale, electrodeposited Ni- and Ni-based alloy coatings are widely used as protective coatings to protect various components against abrasion and corrosion. Pure nickel shows good corrosion resistance in corrosive environments as a coating material but cannot be used effectively to protect components subject to wear due to its low strength and hardness. The hardness, wear and corrosion resistance of the coatings alloyed with metals with high specific properties are significantly increased. Alloy elements and their combination of microstructural changes increase the hardness of alloy coatings. This can be explained by the fact that the fine dispersion in the nickel matrix and grain boundary in the alloying mechanism with metallic elements increases the hardness of the material. Recently, the superior hardness, corrosion, and wear resistance properties of alloy coatings such as Ni-P [1], Ni-B [2], Ni-Cr [3], Ni-W [4], Ni-Fe [5], Ni-Mo [6], and Ni-Co [7] have been investigated for different industrial applications. Among Ni-based alloy coatings, Ni-B coatings are being researched more due to their high strength and excellent corrosion resistance. In addition, Ni-B coatings increase the strength because of the formation of hard Ni_3B intermetallic fine precipitates by heat treatment. For this reason, the hardness of the Ni-B alloyed composites obtained by the dispersion of ceramic particles in the Ni-B alloy matrix is further increased [8,9]. Different reinforcing particles are included to the alloy matrix to increase the strength of the alloy coatings and improve their anticorrosion capability. Studies have been investigated to increase the strength and improve their anticorrosion capability of composite coatings such as Ni-P-$Ti_3C_2T_x$@TiO_2/MoS_2 [10], Ni-B/Al_2O_3 [11], Ni-W/TiB_2 [12], Ni-W/SiC [13], Ni-B/TiC [14], Ni-B/YZS [15], Ni-Cu/TiN [16], and Ni-W/TiN [17] produced with the distribution of hard ceramic reinforcements in Ni-based alloy matrix. Recently, titanium nitride (TiN) reinforcement particles included to the deposited Ni-based alloy coatings have become the focus. Li et al. [18] stated that TiN ceramic particles could be strengthen the hardness and wear resistance of the material in alloy or ceramic matrix applications due to its high hardness, high melting point and thermal stability. Cui et al. [19] stated that TiN particles are uniformly dispersed in the coating, improving the hardness and corrosion resistance of the coating. Because of these considerations, TiN-containing composite coatings are expected to have good prospects for mechanical, abrasion, and corrosion properties. Although there is much literature study about Ni-B composite coating, there has been no research on the coating structure, surface morphology, hardness,

CONTACT Fatih Doğan drdoganfatih@gmail.com

wear, and anticorrosion capability depending on the current density change by the PED method of TiN reinforced Ni-B composite coatings. In this study, the effect of the current density parameter on the pulse electrodeposition method for the Ni-B/TiN composite coatings was investigated to obtain a coating with a dense and uniform structure, high hardness, and excellent wear and corrosion resistance.

2. Experimental methods

2.1. Preparation of Ni-B/TiN composite coatings

The composition and coating conditions for the Watts nickel bath are given in Table 1. 60 mm × 40 mm pure nickel plate was used for the anode, while a mild steel sheet of 40 mm × 30 mm was used for the cathode. During coating, the distance between the anode and cathode was fixed to be 30 mm. Before deposition, the mild steel sheets were polished with metallographic sandpapers in the range of 400–1200 meshes. The sheets were washed in alcohol for 15 minutes with ultrasonic agitation and then rinsed with distilled water at room temperature. The substrate was activated in a 10 vol.% hydrochloric acid solution for 15 seconds and rinsed with acetone and distilled water, then instantly immersed in the coating solution. Before starting the pulse electrolytic coating, the pH of the bath was fixed and controlled during deposition at 3.5. The TiN particles were dispersed by ultrasonic agitation for 30 minutes before being added to the coating solution, followed by magnetic stirring for 1 h at 450 rpm to suspend the particles. Before the PED process the submicron-sized TiN particles at 15 g/L concentration in the electrolyte were mixed with the 0.1 g/L sodium dodecyl sulfate (SDS) surfactant with a magnetic stirrer for at least 30 minutes to suitably disperse and suspend TiN particles in the electrolyte. The zeta potential of particle suspended electrolytes with 0.1 g/L SDS was determined by the Malvern device (Zeta Seizer) for 15 g/L TiN concentration. After providing the suspension of the TiN particles in the Watts bath electrolyte solution, the electrodeposition process was started according to the previously set coating parameters (Table 1). In this work, the parameter value of applied pulse frequency (f) is 100 Hz. To investigate the effects of I_{av} (1.5, 3.0, 4.5, and 6 A/dm^2) parameters on the coating process, other parameter values were kept constant. The relationship between the variables is as follows:

$$f = \frac{1}{T_{on} + T_{off}} \tag{1}$$

$$r = \frac{T_{on}}{T_{on} + T_{off}} x100\% \tag{2}$$

$$I_{pe} = I_{av} x \frac{1}{r} \tag{3}$$

$$I_{av} = I_{pe} x r \tag{4}$$

where f is frequency, r is duty cycle, I_{pe} is peak current density, I_{av} is average current density, T_{on} is current on time (s), and T_{off} is current off time (s).

Table 1. Chemical composition and working parameter of the bath of Ni-B/TiN composite coating produced by electrodeposition.

Electrolyte Composition	
Chemicals	Composition
$NiSO_4.6H_2O$ (g/L)	240
$NiCl_2.6H_2O$ (g/L)	45
H_3BO_3 (g/L)	30
TMAB (Trimethylamineborane) (g/L)	3
SDS (Sodium dodecyl sulfate) (g/L)	0.1
TiN (g/L)	15
Operating conditions	
pH	3.5
Temperature (°C)	50
Current density (A/dm^2)	1.5, 3.0, 4.5, 6.0
Duty cycle (%)	40
Frequency (Hz)	100
Agitation rate (rpm)	450
Deposition time (min.)	60
Anode	Pure Ni
Cathode	Mild Steel

2.2. Characterization of Ni-B/TiN composite coatings

The surface and cross-sectional images of Ni-B/TiN composite coatings were examined using both FESEM, FEI Quanta FEG 450 and JEOL 6060LV scanning electron microscopes. The average surface roughness of composite coatings was measured from five different regions of the samples using a non-contact surface profile. Elemental Ti, N, and B contents were obtained using SEM-coupled Energy Distributor Spectrometry (EDS) and Inductively Coupled Plasma (ICP) spectrometry, respectively. The structure was calculated using XRD (Rigaku D/MAX 2000 X-ray generator and diffractometer) with Cu Kα radiation (1.54059A°). The measurements were collected in 1° (2θ) steps at 1 min per step 20 < 2θ< 80◦. Crystallite dimensions were calculated according to Equation 5 by using Debye-Scherrer formula with full widths at half maximum (FWHM) values of X-ray diffraction.

$$d = \frac{0.9\lambda}{\beta \cos\theta} \tag{5}$$

Where, d is mean crystalline size, λ is X-ray wavelength (0.15418 nm), β is the corrected peak width at half maximum intensity (FWHM) and θ is Bragg diffraction angle. After the composite coatings deposited on the substrate were annealed at 400°C for 1 h, their mechanical and tribological properties were examined. The Nano hardness of the composite coatings under a maximum load of 50 mN for 10 seconds was calculated with the Vickers Nano hardness determinant

(Anton Paar Nanoindentation tester: NHT^3). The hardness of each composite coating was measured from five different regions of the cross-sectional area and the average value was calculated. The tribological behavior of coatings in a sliding against steel ball at room temperature and ambient humidity under dry sliding conditions on a Tribometer (CSM Instruments TRB 18–317) was investigated. The wear tests of composite coatings against an Al_2O_3 ball (Ø 6 mm) were performed from 5.0 N load with sliding speeds of 40 cm/s. and total 750 m sliding distance was chosen. The wear rates and coefficients of friction of the coatings were calculated after the wear tests applied to the heat-treated composite coatings. Wear surfaces of composite coatings were analyzed with low and high magnification micrographs using SEM. 3D profiles of wear traces were examined using KLA Tencor-P6 surface profile measuring device. Tafel electrochemical tests were performed in a three-electrode cell for corrosion calculations with wt.% 3.5 NaCl solution; graphite was used as the counter electrode, saturated Calomel Electrode (SCE) for the reference electrode and Ni-B/TiN composite coating for a working electrode. Potentiodynamic polarization measurements were calculated by scanning the potential between −1.0 V and +1.0 V at a scan rate of 1 mV s^{-1} at ambient temperature using the Gamry Reference 3000 Potentiostat model computer. Corrosion potentials (E_{corr}) and corrosion currents (i_{corr}) were calculated using the Tafel curves. Electrochemical impedance (EIS) analyzes were measured with a signal of 10 mV amplitude applied to the electrode in the frequency range of 0.1 Hz–100 kHz. After the corrosion tests, morphologies of the coatings were characterized by SEM.

3. Results and discussion

3.1. Morphology of Ni-B/TiN composite coatings

SEM images of Ni-B/TiN composite coatings prepared at *Ia* = 1.5, 3.0, 4.5, and 6.0 A/dm^2 are shown in Figure 1. It is observed that the incorporated TiN particles in the matrix at low current densities (1.5 A/dm^2 and 3.0 A/dm^2) are distributed nonuniformly and protruding structures are formed by the preferential particles accumulating on the deposited Ni-B grains (Figure 1 (a,b)). This may be attributed to the low surface energy of the TiN particles that reaching to the cathode surface were separated from the metal matrix on the

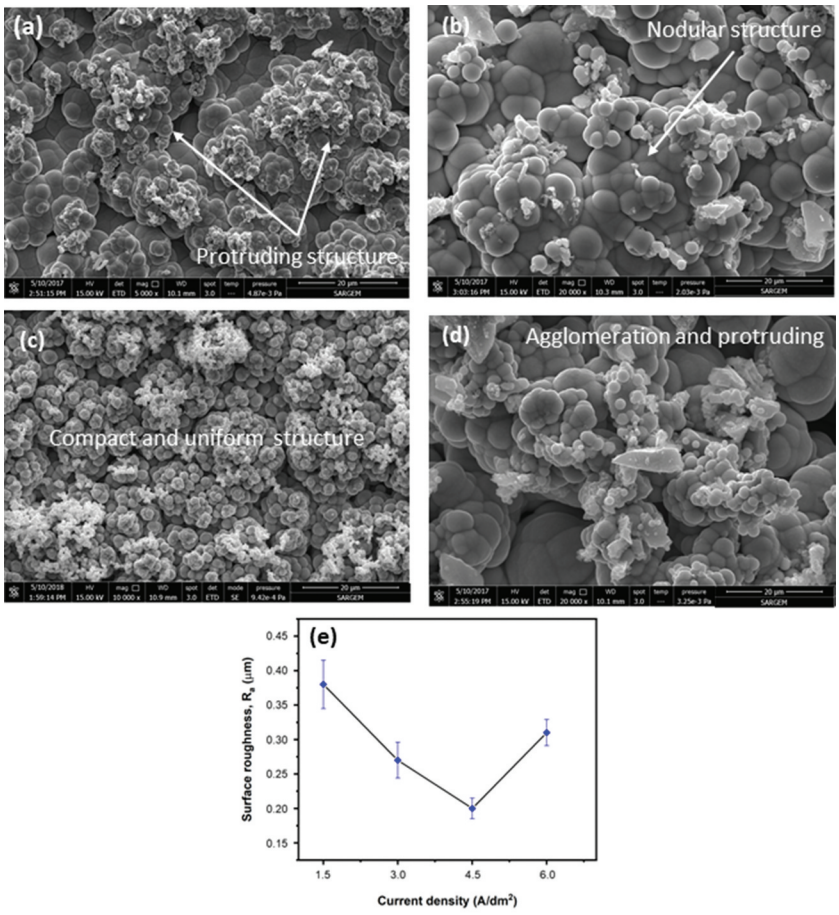

Figure 1. Surface SEM images of Ni-B/TiN composite coatings produced at different current densities: (a) 1.5 A/dm^2, (b) 3.0 A/dm^2, (c) 4.5 A/dm^2, and (d) 6.0 A/dm^2, respectively. (e) Surface roughness values of TiN reinforced Ni-B composite coatings at different current densities.

substrate [20]. In contrast, when the current density is increased to 4.5 A/dm^2, the protrusions and gaps on the cathode surface decreased. Moreover, as shown in Figure 1(c) at 4.5 A/dm^2, the surface of coating is more compact, and the TiN particles are homogeneously distributed on the coating surface. Moreover, the TiN particles settled on the interfaces between grains of the Ni-B alloy matrix and the particles adsorbed uniformly onto the nodular structure, thereby reducing the protruding structures of the coating surface [21]. Similarly, Radwan et al. [22] described the inclusion of particles in the nickel-based matrix as their adsorption to the cathode surface with Van der Waals attractive forces and named the binding of particles with nickel ions as mechanical locking. At higher current densities (6.0 A/dm^2), the movement of metal ions toward the cathode surface could accelerated due to the increase in electric field force which result in occurring coarse surface morphology because of different deposition rates. Since the movement of the particles are supported, the amount of particles moving to the cathode surface increases. On the other hand, the amount of particles incorporated into nickel matrix is decreased since the reduction rate of nickel ions in a region with high current density is higher than the deposition rate of the particles. In addition, as seen in Figure 1(d), the particle agglomeration formed on the coating surface could be explained by the poor dispersion of TiN particles in the electrolyte at high current density [23]. The average surface roughness (Ra) of composite coatings measured using a noncontact surface profile was chosen from five different regions of each sample and is shown in Figure 1(e). Surface roughness and surface morphology varied depending on the different current densities of the composite coatings. Considering the increase in TiN particle content with increasing current density in the composite coating, which will be described later, with the increase of current density in the coating, the ceramic particles in the matrix are distributed evenly and the roughness of the coating surface is decreased. Similarly, Xu et al. [24] elucidated that increasing the particle concentration in the composite coating performed the coating surface smoother. The reason obtaining compact surface and fine grain structure has been attributed to the heterogeneous nucleation effect. This can be explained that more nucleation sites on the nickel matrix would be available at current density of 4.5 A/dm^2 and the roughness was decreased to 0.22 µm. However, further increase in the current density (6.0 A/dm^2) results in increasing rougher surface from 0.22 µm to 0.32 µm.

Cross-sectional SEM images of composite coatings deposited at different current densities are shown in Figure 2. It is seen that the substrate/coating interface has a crack-free structure in all the composite coatings which shows a well adhesion has been achieved during depositions. The results reveal that the amount of incorporated ceramic particles and thickness of coatings is strongly affected by current density. It was already stated in the literature that the high reduction of metallic ions on the cathode in the early stages of the electrodeposition process affects the coating thickness and the particle content [25]. As the current density is increased, the thickness of coatings increased. Accordingly, TiN particles surrounded by ions, which are rapidly transported to the cathode surface at high current density, result in increasing the thickness of Ni-B alloy coating. It is observed that the content of TiN particles incorporated into Ni-B alloy matrix at low current densities is low and the coating thickness is between ~22 µm and ~58 µm for 1.5 A/dm^2 and 3.0 A/dm^2 current densities respectively. This can be due to slow movement of metallic ions reaching the cathode surface at low current densities (Figure 2(a,b)). Agglomeration of TiN particles is seen a significant problem form low current density depositions. In cross-sectional views of the composite coating deposited at a current density of 4.5 A/dm^2, TiN particles are seen to be distributed more homogeneously than other coatings and the coating thickness increases to

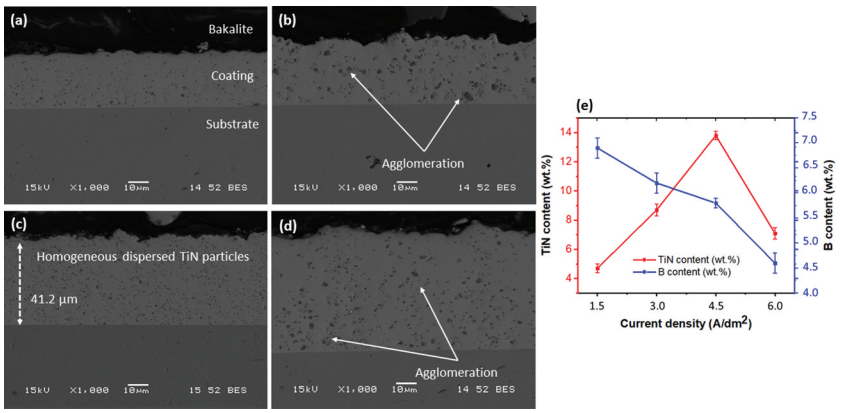

Figure 2. Cross-sectional SEM micrographs of Ni-B/TiN composite coatings produced at different current densities: (a) 1.5 A/dm^2, (b) 3.0 A/dm^2, (c) 4.5 A/dm^2, and (d) 6.0 A/dm^2, respectively. (e) Change of B and TiN content in the coating depending on the current density.

~41.2 μm (Figure 2(c)). Despite thickness increment at the 6.0 A/dm^2 current density deposition condition, there seems a strong agglomeration of TiN particles (Figure 2(d)). Figure 2(e) exhibits TiN particle and boron content in the alloy matrix versus current density. Also, it indicates that the TiN amount in nickel matrix increased with increasing the current density from 1.5 A/dm^2 to 4.5 A/dm^2, but then decreased with further increasing above 4.5 A/dm^2. It can be concluded that increasing the current density leads to increase the deposition rate of the Ni-B/TiN composite coatings. From the cross sectional micrographs given in Figure 2, as also reported by Zhou et al [26] it can be stated that the particles adsorbed to the cathode surface are increased with the increase in the deposition rate in the coating as the nucleation center and the coating thickness increases. As was known, the adoption of particles surrounded by metal ions to the substrate surface and reduction of metal ions to the cathode surface depends on the particle transport in the electrolyte [27]. Therefore, at low current densities could be explained by the high metal matrix formation on the cathode surface due to the precipitation of the Ni and B elements rather than reduction on the TiN particles. Another reason the reduction of the particle content in the composite coating may be due to the deposition rate of the nickel ions higher than the diffusion rate of the TiN particles at high current density. Nevertheless, the reduction rate of Ni ions increases as the ion transfer migrating to the cathode surface increment with increasing current density during electrodeposition. Alizadeh and Cheshmpish [28] explained that the particle content incorporated in the coating at high current densities was lower compared to the low current densities by increasing the reduction rate of metal ions and decreasing the deposition of particles at high current densities. On the other hands, it was seen that the B content in the alloy matrix decreases with the increase in the current density in the Ni-B/TiN composite coatings. When the current density is increased to 4.5 A/dm^2, the electrophoretic repulsion force effect increases the TiN particle content in the composite coating, thereby limiting the deposition of B ions with Ni ions. By further increasing the current density, the TiN particles in the electrolyte interact more with the effect of the high current density to form agglomerates. Thus, bigger size TiN particles incorporated in the coating was prevented the deposition of boron ions. Mehr et al. [29] also stated that the boron content in the matrix alloy decreases with the increase at current density in Ni-B composite coating with particle reinforcement.

3.2. Effect of current density on phase constituent and crystallite size

The effect of current density on the structure of Ni-B/TiN composite coatings after heat treatment at 400 C for 1 h is shown with XRD patterns in Figure 3(a). The reflections have a face centered cubic (fcc) nickel structure and the crystal planes in all coatings are: (111), (200) and (220) planes for 44.51°, 51.84°, and 76.37° 2θ angles are detected, respectively. The XRD patterns of TiN given with (111), (200), and (220) planes for 37.16°, 42.79°, and 61.62° 2θ angles are observed. The peaks corresponding to the TiN cubic structure are very close to the values obtained in the literature [30]. In addition, Ni_2B and Ni_3B phases are observed after heat treatment. The dominant preferential growth of Ni crystals appears to be in the (111) plane. It could be stated that with the change of current density in electrodeposition, the increase of TiN particle content in the alloy

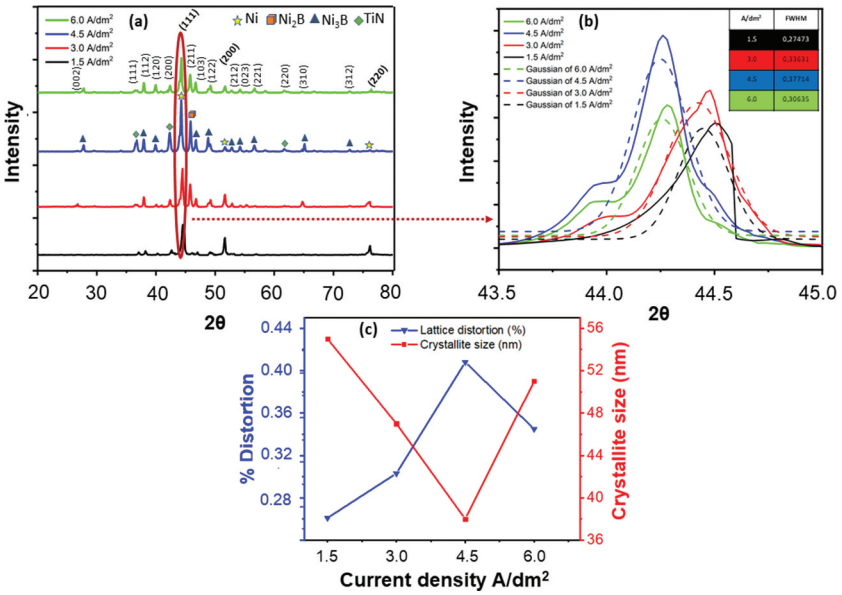

Figure 3. (a) XRD patterns, (b) diffraction peak broadening from (111) plane, (c) lattice distortion and average crystallite sizes of electrodeposited Ni-B/TiN composite coatings produced at different current densities.

matrix promoted the preferential growth of Ni crystals in the (111) plane. As seen in the Figure 3(a), as the current density of the coating increases up to 4.5 A/dm^2, the intensity of the diffraction peaks (220), (200) decreases slightly, whereas (111) the diffraction peak increases (at 4.5 A/dm^2) and then decreases by further increase in the current density (at 6 A/dm^2). Figure 3(b) shows the peak shifting for the (111) peak at narrow 2θ angle depending on the current density. The full width at half maximum (FWHM) for Ni (111) peak in composite coating produced with 4.5 A/dm^2 was wider than other coatings. The increase in the particle content in the coating with the increase in current density causes to peak broadening which leads to decreasing the crystallite size of coating. The lattice distortion and crystallite size of composite coating deposited with different current densities are shown in Figure 3(c). According to the FWHM of Ni (111) peaks, the crystallite size of Ni-B composite coating could be calculated according to the Scherrer equation and as it is seen from Figure 3(a), by increasing the current density, first the crystallite size of the coating is decreased from 55.8 nm to 37.4 nm and then increased to 51.3 nm for 6.0 A/dm^2 coated composite. The lowest crystallite size was obtained at composite coating deposited at a current density of 4.5 A/dm^2. This can be explained by the highest content of codeposited TiN particles in the Ni-B alloy matrix by supporting the nucleation areas of the crystals, preventing the growth of existing crystals, which is consentient with results reported by Mirzamohammadi et al [31]. The reduction of the crystallite size of the coating leads to the development of mechanical properties such as hardness and abrasion resistance [32]. The lattice distortions of samples produced at different current densities are shown in the Figure 3(c). The lattice constant could be calculated for an fcc systems as follow:

$$a^2 = \left(\frac{\lambda^2}{4sin^2\theta}\right)\left(h^2 + k^2 + l^2\right) \tag{6}$$

The deflection in the lattice constant was calculated using the following equation:

$$LatticeDistortion\% = 100\left(1 - \frac{a_1}{a_0}\right) \tag{7}$$

where, a_1 is the lattice constant for composite coatings produced with different current densities, a_0 is the lattice constant of Ni. The lattice distortion values were calculated using Equations (6) and (7). Low-angle grain boundaries due to dislocations and lattice distortion are associated with grain refinement in the crystal structure [33]. As the current density increased, negative lattice distortions occurred in the Ni matrix. Negative lattice distortion in particle reinforced MMCs could be explained in terms of lattice parameter mismatch, thermal stresses, and residual stress [34]. As previously discussed in the XRD analysis, with increasing current density decreased the intensity of the crystal plane (200) and (220), increased the intensity of the (111) plane. Reinforcement particles added to the Ni-B alloy matrix can cause lattice expansion or contraction due to its chemical bond. Depending to the increased current density, TiN particles penetrate the Ni-B matrix, increasing the lattice disruption of nickel. The lattice degradation of the composite material is explained by the lattice mismatch between the substrate interface and the coating. The other reason is residual or actual stresses from certain coating conditions [35].

3.3. Effect of current density on mechanical properties

Nanoindentation measurements of composite coatings were tested from cross-sectional microstructures of samples. As it is known, the penetration depth in the nanoindentation technique has great importance in comparing the mechanical properties of the coatings. The Berkovich indenter penetrates the sample until prespecified maximum load (plastic deformation) was reached during indentation process. Unloading (elastic deformation) displacement which that zero load was reached, and final residual depth was measured when indenter was retracted from sample [36]. The mechanical properties of Ni-B/TiN composite coatings deposited at different current densities are shown in Figure 4. Obviously, the hardness of Ni-B composite coating firstly increased with the increase of current density from 1.5 A/dm^2 to 4.5 A/dm^2, then decreased with further increasing current density from 4.5 A/dm^2 to 6.0 A/dm^2. For example, while the hardness value of the coating deposited at 1.5 A/dm^2 current density is ~800 HV, when the current density is increased to 4.5 A/dm^2 the composite coating hardness increased by approximately 56.8% and the value of ~1210 HV has been accomplished. The increase in the coating hardness can be attributed to the higher hardness of TiN particles with the increase of their content. In addition, the increase in hardness can be explained by the fact that the particles prevent the dislocation movement and contribute the resistance against plastic deformation. In literature, the increase in coating hardness was explained by matrix grain refinement (Hall-Petch) and reinforcement phase hardening (Orowan) mechanisms [24]. In addition, dislocation movement that prevents the growth of existing crystals was prevented, as the excessively distributed TiN particle content in the coating reduce the distance between the particles in the high content of particle codeposited composite coatings [37]. Tao et al. [38] stated that Ni-B coating hardness increases with solid solution reinforcement and fine grain strengthening effects. They also explained that the increase in coating hardness was related to the formation of hard Ni_3B phases formed after heat

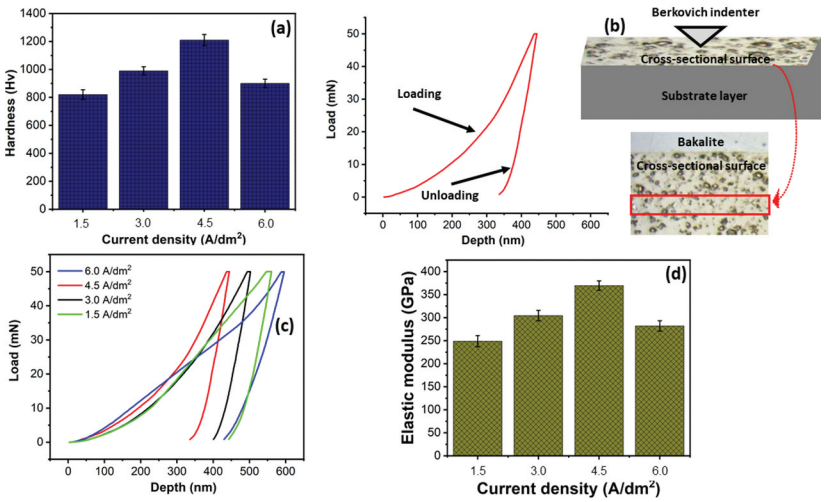

Figure 4. (a) Hardness, (b) elastic modulus, (c) load-depth curves for Ni-B/TiN composites produced at different current densities, and (d) schematic diagram of hardness measurement, respectively.

treatment. In addition to these, when the coating thicknesses indicated in Figure 2 are taken into consideration, it can be said that the reinforcement particles distributed homogeneously to the Ni-B alloy in the coating (41.2 µm) deposited at a current density of 4.5 A/dm^2 evenly adsorb the applied load and affect the increase of the coating hardness. On the other hand, when the current density is increased to 6.0 A/dm^2, the reduced hardness despite the increased coating thickness can be associated with the low content of TiN particles embedded in the coating and the agglomeration of the particles. Using the Berkovich diamond indenter tip by the Oliver Pharr method, the nanoindentation measurements of the coatings with a max. 50 mN indentation force are shown schematically in Figure 4(b). The loading-unloading curves obtained using the nanoindentation technique in the composite coatings deposited at increasing current densities are shown in Figure 4(c). The absence of bending in the nanoindentation curves proves that the coatings are crack-free. According to the results, it is seen that the nanoindentation curve of the coating deposited at 1.5 A/dm^2 current density has higher penetration depth than the other coatings. It could be stated that with the increase in the current density (4.5 A/dm^2), the particles in the coating improve the resistance against indentation, reducing the depth of the indent penetration to ~330 nm, thereby increasing the mechanical properties of the coating. At 6.0 A/dm^2, the indentation depth increased more than 1.5 times and reached ~440 nm. According to the elastic modulus results (Figure 4(d)) obtained from the nanoindentation tests, the elastic modulus of the coating increased up to 370 GPa with the increase in the current density then decreased with further increasing current density from 4.5 A/dm^2 to 6.0 A/dm^2. As known, hard coatings undergo less plastic deformation during loading, while soft coatings were exposed to larger plastic deformation [39]. Accordingly, the high elastic improvement of hard Ni-B/TiN composite coatings could be attributed to the increase in reinforcement TiN particle content in the coating with the current density parameter in electrodeposition.

3.4. Dry sliding wear properties of composite coatings deposited at various current densities

Tribological properties of heat-treated Ni-B/TiN composite coatings deposited on the steel substrate were examined by dry sliding wear tests. Wear rates and coefficient of friction (COF) values of Ni-B/TiN composite coatings produced variation current density are shown in Figure 5. The COF values shown in Figure 5 (a) change from 0.16 to 0.20, and with the increase in current density, the friction coefficients decreased and then increased. Friction coefficient of the Ni-B/TiN composite coating prepared at 3.0 A/dm^2 decreased remarkably compared to those Ni-B/TiN composite coating produced at 1.5 A/dm^2 and friction coefficient of the composite coatings exhibited a decreasing trend with the increase in the current density. Among the four Ni-B co-depositions, Ni-B-TiN composite coating deposited at 4.5 A/dm^2 exhibits the lowest friction coefficient, 0.16, which is nearly 6%, 18%, and 25% lower than that of the Ni-B/TiN composite coating deposited at 1.5, 3.0, and 6.0 A/dm^2, respectively. For composite coating deposited at 4.5 A/dm^2, TiN particles carrying the load during wear resulting in reduce the friction coefficient because the ceramic particles are uniformly dispersed in the Ni-B alloy matrix and decreased the distance between the particles [40]. The increased friction coefficient at higher current density could be attributed to the low TiN particle content in

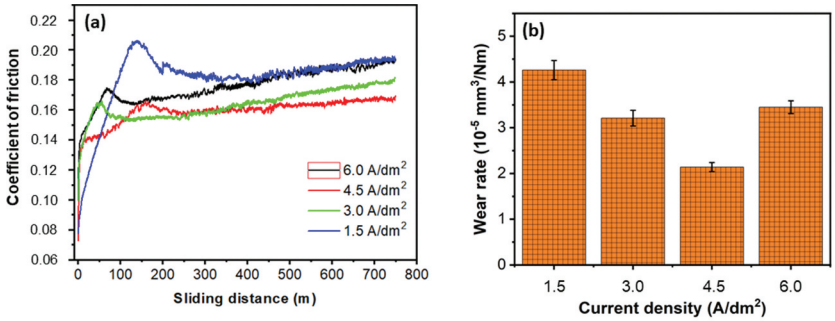

Figure 5. Effect of composite coating deposited with different current density on (a) coefficient of friction and (b) wear rate.

the coating and consequently to the low hardness in the coating. As seen in Figure 5(a), the wear rate of Ni-B/TiN composite coating firstly decreased with the increase of current density from 1.5 A/dm^2 to 4.5 A/dm^2, then increased with further increasing current density from 4.5 A/dm^2 to 6.0 A/dm^2. For example, compared to the wear rate of composite coating (3.21×10^{-5} mm^3/Nm) deposited at 3.0 A/dm^2, the wear rate of the composite coating deposited at 1.5 A/dm^2 significantly high, which is of 4.26×10^{-5} mm^3/Nm. When the current density is increased to 4.5 A/dm^2, the wear rate of the coating decreased to 2.14×10^{-5} mm^3/Nm nearly two times lower than that of composite coating deposited at 1.5 A/dm^2. Wasekar et al. [41] reported that the particle content in the composite coating affected the wear rate of the coating. Accordingly, the reduced wear rate in the Ni-B/TiN composite coating can be attributed to increased hardness by increasing the content of ceramic particles in the matrix. Also, the decreasing in wear rate could be explained by reducing the contact area between the coating/counter-surface of TiN particles adsorbed to the coating surface. Moreover, the increased current density in the cross-sectional view of the composite coating indicated in Figure 2(c) and the proximity of the particles in the coating could be attributed to the equal bearing of the load during wear. When the current density in the coating solution is further increased, the particles agglomerate on top of each other in the alloy matrix due to the increasing electrophoretic force. Thus, at the 6.0 A/dm^2 current density, the wear rate of the coating increased to 3.45×10^{-5} mm^3/Nm due to the insufficient particles to reduce the contact between the abrasive surface and the coating. As a result, the TiN particles in the Ni-B alloy matrix in parallel with the hardness/wear rate relation specified by the Archard relationship in the literature increased the hardness of the composite coating and reduced the wear rate of the coating [28].

Figure 6 exhibits the worn surfaces of composite coatings produced with various current densities. As seen from Figure 6(a-c-e-g), the width of wear track continuously decreases when current density increases from 1.5 A/dm^2 to 4.5 A/dm^2 but then starts to increase with further increase from 4.5 A/dm^2 to 6.0 A/dm^2 due to because of the agglomerated ceramic particles. For example, at 1.5 A/dm^2, the wear track width of the coating is observed to be wide compared with the coating deposited at 3.0 A/dm^2 due to the low hardness of the coating and weak adsorption of particles depositions on the coating surface at low current densities in the coating process. As seen in Figure 6(e), the wear trace width (456 µm) of the coating deposited by increasing the current density to 4.5 A/dm^2 is narrower than the other coatings. This could be explained by the uniform adsorption of TiN particles with hard properties on the coating surface and thus low irregularities on the coating surface. Moreover, for composite coating deposited with 1.5 A/dm^2, microcracks are observed on the worn surfaces because high shear stress is located on the surface during the wear test, showing typical rough appearance of adhesive wear and fatigue wear cracks, which is in agreement with its high wear rate [42]. When the applied current density is raised to 3.0 A/dm^2, the microcracks significantly reduced and island-like layer is observed in Figure 6(d). However, when the current density increased to 4.5 A/dm^2, a smooth layer and small smeared flakes can be shown on the worn surface. On the other hand, crack formation and initiation at worn surface seems to be minimal for composite coating. Therefore, it is concluded that with increasing current density which increased incorporated particle amount in the matrix prevents dislocation movement and increases the plastic deformation resistance and load bearing capacity of Ni-B alloy matrix [26]. For the composite coatings deposited at 6.0 A/dm^2, microcrack, and spall from wear tracks shown on worn surface because of high plastic deformation. Therefore, the cracks formed on worn surface would grow along the interface, and then leads to delamination. This may be attributed to both low amount of TiN particles and severe particle agglomeration in the coating at high current density. As also stated before, the surface roughness of the composite deposited at 6.0 A/dm^2 was high and it is thought high surface roughness is another significant reason to lead the local plastic deformation caused by high shearing. Thus, the decrease in the amount of

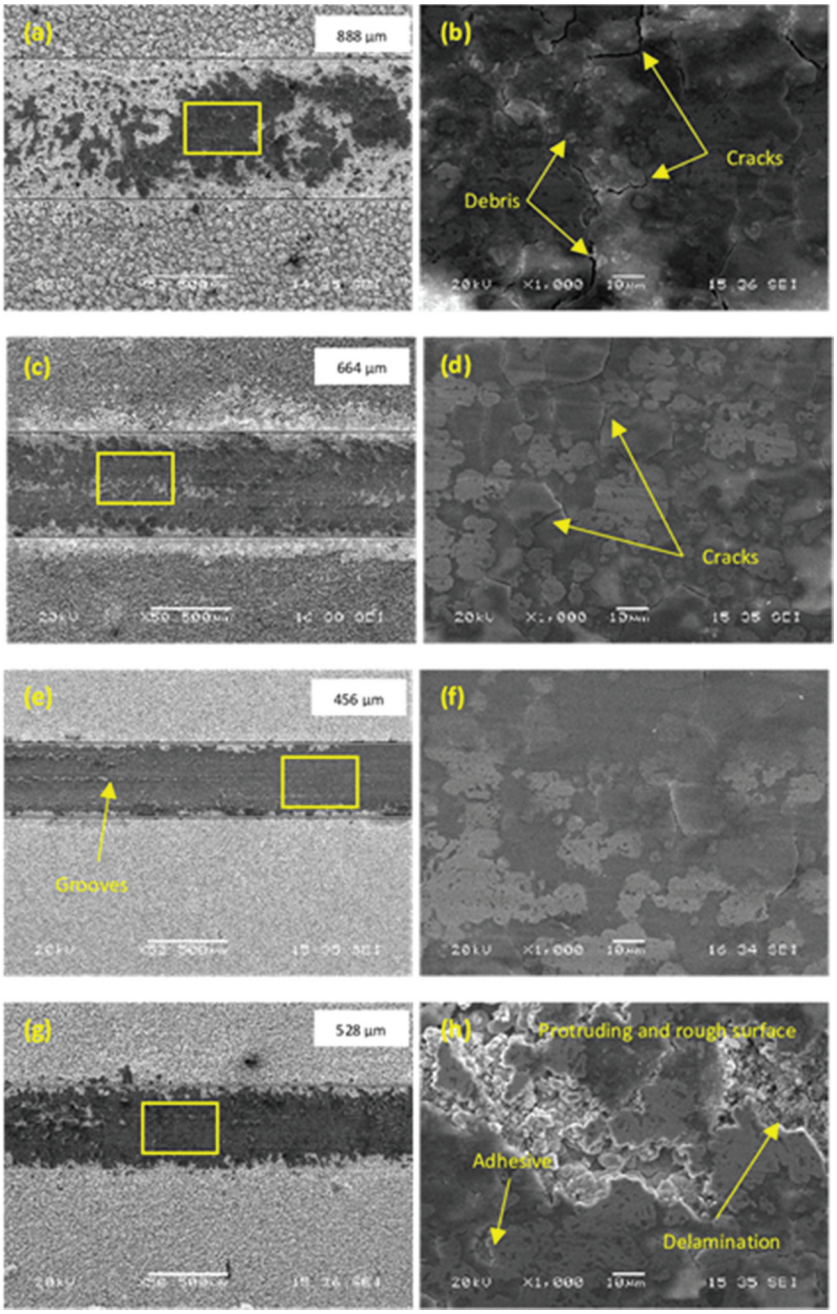

Figure 6. Low and high magnification SEM images of wear tracks for the Ni-B/TiN composite coatings deposited at different current densities: (a and b) 1.5 A/dm^2 and (c and d) 3.0 A/dm^2, (e and f) 4.5 A/dm^2, and (g and h) 6.0 A/dm^2.

particles incorporating in the nickel matrix and high plastic flow because of shearing, weak interfacial bonding between ceramic particles and nickel matrix emanated from segregation lead to the wear rate.

The worn surfaces of composite coatings were scanned with 3D profilometry to get a better understanding the effect current density on wear mechanisms of composite coatings deposited at different current densities. The results of 3D profilometry for composite coatings are shown in Figure 7. The surface roughness at low current density (1.5 A/dm^2) seems to show a decreasing tendency when the current density is increased to 3.0 A/dm^2. When the current density is increased to 4.5 A/dm^2, it is seen that the roughness of the wear surface decreases due to the increase of particle content in the matrix. As stated before, because of high particle content co-deposited during Ni-B coating, resulted to produce smoother surfaces. High particle content in the deposited layer leads high nucleation and low growth rate of the matrix and therefore causes to reveal dense and low surface roughness structure. It is concluded that The Ni-B composite coating deposited at 4.5 A/dm^2 exhibits very smooth surfaces compared with composite coatings produced at 1.5 A/dm^2, 3.0 A/dm^2, and 6.0 A/dm^2. Thus, it could be stated that surface damage and plastic deformation on the wear surface were reduced [43]. It can also be noted that increasing coating thickness with increasing current density affects the wear surface. Accordingly, the fact that the abrasion scar depth

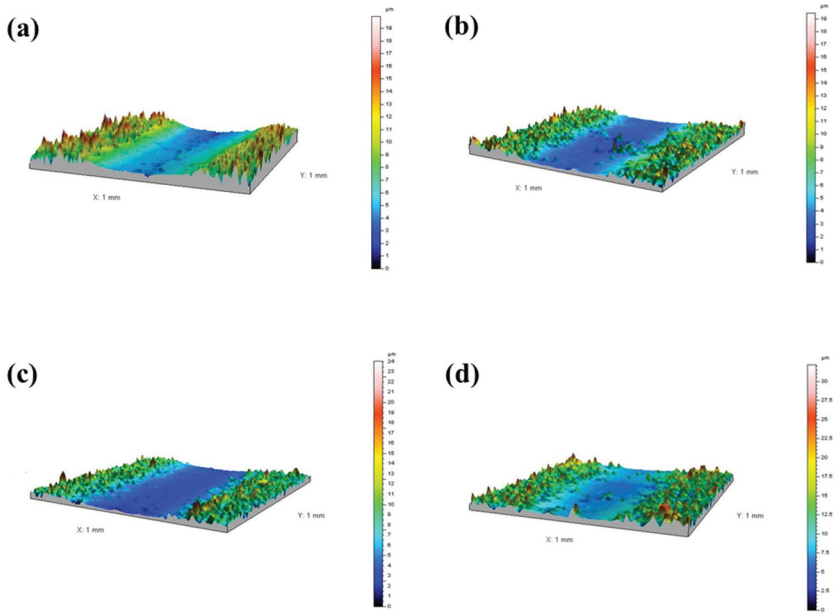

Figure 7. 3D profilometry results of Ni-B/TiN composite coatings: (a) 1.5 A/dm^2 and (b) 3.0 A/dm^2, (c) 4.5 A/dm^2, and (d) 6.0 A/dm^2.

in the coating produced with 4.5 A/dm^2 current density is lower than the other samples can be explained by the fact that the particles on the coating surface form a protective layer and the particles in the coating are close to each other. It can be seen from Figure 7, The Ni-B composite coating deposited at 6.0 A/dm^2 has very rough surface that indicating a severe surface damage occurred. This can be attributed to although the further increasing current density also increases the coating thickness, the uneven distribution of the low amount of particles in the coating.

3.5. Effect of corrosion behavior on current density

The corrosion behavior of Ni-B/TiN composite coatings deposited at different current densities were analyzed by Tafel curves and EIS measurements. Figure 8(a) shows the potentiodynamic polarization curves of Ni-B/TiN composite coatings produced at different current densities in 3.5 wt.% NaCl solution for 1 h. E_{corr}, i_{corr} and r_{corr} values calculated by Tafel method are presented in Table 2. As shown in the Figure 8(a), the E_{corr} value shifts toward the positive direction by increasing the current density to 4.5 A/dm^2. i_{corr} value also decreases to 1.1 × 10^{-6} A/cm^2 It was stated that the uniformly dispersed ceramic particles in the nickel matrix could prevent corrosion by form a physical barrier between the coating and the corrosive environment [24]. What's more, TiN particles could have prohibited ion diffusion from the corrosive medium by filling defects in the coating structure such as porous and gap. In addition, the reinforced particles dispersed in the Ni-B alloy matrix cause to increase the

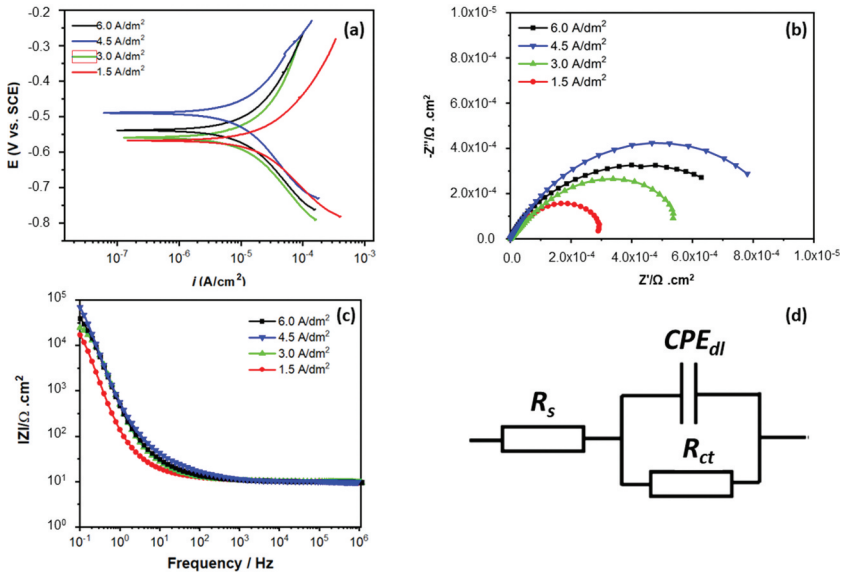

Figure 8. (a) Potentiodynamic polarization curves, (b) Nyquist plots, (c) Bode plots of Ni-B/TiN composite coatings at different current density that were electrified in 3.5 wt.% NaCl aqueous solution. (d) Equivalent electrical circuit model.

Table 2. Corrosion potential (E_{corr}) and corrosion current density (i_{corr}) values of Ni-B/TiN composite coatings produced at different current densities.

Current density (A/dm^2)	i_{corr} (A/cm^2)	E_{corr} (V)	r_{corr} (mm.y^{-1})
1.5	1.7×10^{-5}	−0.565	0.0670
3.0	3.6×10^{-5}	−0.551	0.0391
4.5	1.1×10^{-6}	−0.492	0.0013
6.0	2.9×10^{-5}	−0.543	0.0207

nucleation regions that its lead to the dense composite structure which prevents Ni dissolution. Therefore, composite coating shows high resistance to corrosion [44]. When the current density is further increased to 6.0 A/dm^2, the i_{corr} value increases to 2.9×10^{-5} A/cm^2. TiN particles in the composite coating deposited at higher current density are insufficient to avoid anodic dissolution and defect corrosion, as the TiN particles could not form a physical barrier on the coating surface. The results show that chemical composition of the bath, the crystallite size of the matrix, and the distribution of TiN particles in the matrix affect the corrosion resistance of the Ni-B/TiN composite coating [45]. The corrosion rates (r_{corr}) of composite coatings has been calculated according to Equation 8 [46] using i_{corr} values:

$$r_{corr} = \frac{kM}{n\rho} i_{corr} \tag{8}$$

where k is the constant (3270 mol A^{-1}), M is the molar mass, n is the charge number, ρ is the density of the substrate. The lowest corrosion rate of the coating is obtained for composite coating deposited at 4.5 A/dm^2. Nyquist and Bode plots were analyzed to examine the corrosion capabilities of composite coatings in more detail. The radius of the different semicircular Nyquist graphics explains the polarization resistance of composite coatings and the anticorrosion capability with the larger radius [18]. As seen in the Figure 8(b), the radius of the largest semicircle is obtained for Ni-B composite coating deposited at 4.5 A/dm^2. TiN particles uniformly distributed over the composite coating surface, increase the corrosion resistance of the coating by creating a layer that prevents the passage of ion (Cl^-) from the abrasive medium to the composite coating [47]. However, when the current density is further increased, the corrosion resistance of the material decreases as the porous structure formed on the surface of the material diffuses from the porous structure due to the increase in the growth rate of the grains in the coating and thus the radius decreases [11]. As seen in Bode-Z graphics, the maximum value of |Z| at 0.01 Hz was obtained in the coating deposited with 4.5 A/dm^2. Since the ions in the corrosive medium can be inhibited from reaching the substrate, the corrosion resistance of the coating with a current density of 4.5 A/dm^2 is better than other coatings. The fact that other coatings that were tested at the same immersion time have structure that is more porous reduces their anticorrosion capacities. The Bode plots confirm the anticorrosion effect of the optimum current density of the composite coating. The electric equivalent circuits in Figure 8(d) were used to calculate the corrosion parameters, the single-time constant model indicated by the impedance diagram. Where R_s is the solution resistance, R_{ct} was charge transfer resistance, CPE_{dl} was electric double layer capacity. The relative radius of the impedance curve could be used to define the corrosion resistance [48]. Corrosion parameters of Ni-B/TiN composite coatings deposited at different current densities after immersion in 3.5 wt.% NaCl solution for 1 h are given in Table 3. With increasing current density in the coating solution, the R_s and R_{ct} values of the coating increase, while the CPE_{dl} value decreases. To evaluate the protective capabilities of composite coatings against aggressive media, diffusion inhibition of R_{ct} has been evaluated. When the current density is increased to 4.5 A/dm^2, the anticorrosion capacity R_{ct} and R_s of the coating reached the maximum value. With the increase in current density in the coating process, TiN particles have accumulated in active places on the coating surface, thereby improving the corrosion protection of the coating. On the other hand, due to the low surface roughness and uniform particle distribution, the reduction of the double layer constant phase element (CPE_{dl}), indicating that the particles form a barrier layer on the coating surface. In addition, the contact area of the corrosive medium/coating interface, which expands due to the high roughness in the coating, could facilitate the passage of corrosive ions into the substrate. Surface images of Ni-B/TiN composite coatings after immersion in 3.5 wt.% NaCl solution for 1 h are shown in Figure 9. Ions that diffuse from abrasive medium to defects such as micro pore on the coating surface cause to corrosion [49]. With increasing current density in the coating process reduced the corrosion defects on the coating surface. As seen in the Figure 9, ions penetrating the micropores on the surfaces of the coatings deposited at low current densities reduce the corrosion resistance of the coating. Although corrosion formations appear on the surface of the coating deposited with 4.5 A/dm^2, it seems that the microstructure has not changed, and the corrosive

Table 3. Corrosion parameters of Ni-B/TiN composite coatings deposited at different current densities after immersion in 3.5 wt.% NaCl solution for 1 h.

Current density (A/dm^2)	R_s (Ω.cm^2)	R_{ct} (kΩ.cm^2)	CPE_{dl} (μF/cm^2)	n-value
1.5	5.83	28.66	96.92	0.856
3.0	6.13	36.47	72.63	0.871
4.5	7.92	49.48	64.51	0.932
6.0	6.54	38.65	70.62	0.908

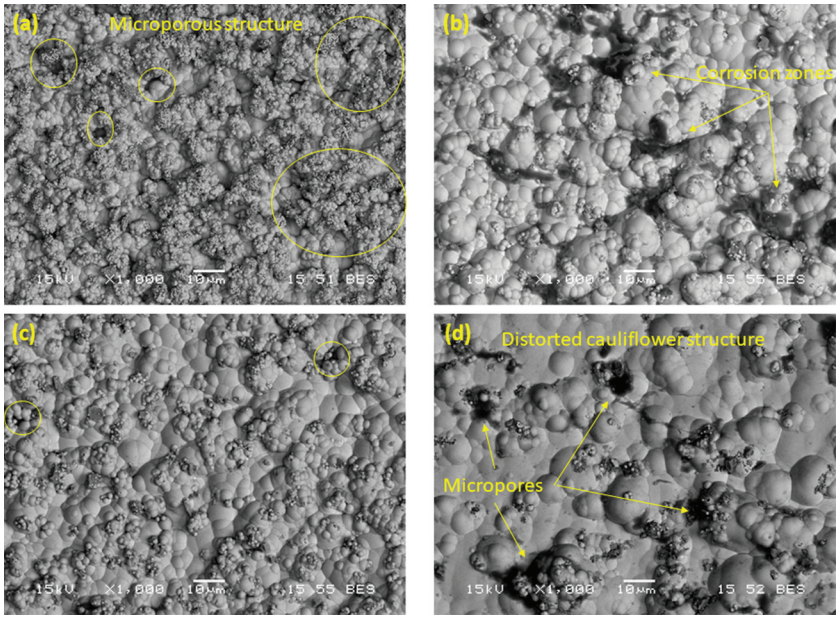

Figure 9. Surface morphology of Ni-B/TiN composite coatings deposited at different current densities after corrosion, respectively.

environment does not cause destruction on the coating surface. TiN particles deposited at 4.5 A/dm^2 current density acted as a physical barrier and limited the diffusion of corrosive ions into the coating. It could also consider that TiN particles improve the anticorrosion capability of the composite coating by preventing corrosion defects. The decreased particle content in the coating deposited at higher current density could be attributed to the corrosion resistance reduction of the coating as it could not fill the gaps on the coating surface and prevent the expansion of the corrosion holes.

4. Conclusions

Ni-B/TiN composite coatings were produced on mild steel plate with different current densities (1.5, 3.0, 4.5, and 6.0 A/dm^2) by pulse electrodeposition method and their effect on surface morphology, phases structure, hardness, tribology, and corrosion properties were investigated. Ni-B/TiN composite coatings are characterized by nodular morphology, crack-free surface, and uniformly distributed TiN in the nickel matrix. The roughness of the coating surface was reduced with the increase of the current density up to 4.5 A/dm^2, beyond which it decreases. As a result of the XRD analysis performed after the heat treatment applied to composite coatings, it was observed that the nickel crystal in the coatings was in the preferential direction in the dominant plane of (111). Considering the effect of current density on the particle concentration in the coating, the minimum crystal size (37.4 nm) and the maximum TiN particle content of the nickel matrix in the coating deposited at a current density of 4.5 A/dm^2 were calculated. Accordingly, it was observed that the elastic modulus and nano-hardness of the coating increased. The wear rate of the composite coating deposited at a current density of 4.5 A/dm^2 was lower (2.14×10^{-5} mm^3/Nm) than other coatings, indicating that the hard-TiN particles reduce the contact area between the coating and the countersurface. Due to the effect of the current density in the electrolyte, the dense structure of the particles deposited on the cathode surface on the composite coating surface prevented the corrosive ions to diffuse into the solution/coating interface by compose a physical barrier. The results obtained from the electrochemical tests exhibited that the Ni-B/TiN composite coatings fabricated at current density of 4.5 A/dm^2 have significant corrosion resistance compared to the other composite coating. The experimental results obtained could be suggested as an alternative composite coating in engineering applications by considering the current density parameter in the coating process of Ni-B/TiN composite coatings.

Disclosure statement

No potential conflict of interest was reported by the authors.

Funding

This work has been supported by the National Boron Research Institute of Turkey (Grant No: 2017-31-07-25-001) and Scientific Research Projects Unit for the Sakarya University (Grant No. 2016-50-02-007), Turkey.

ORCID

Fatih Doğan http://orcid.org/0000-0002-4234-4034
Erhan Duru http://orcid.org/0000-0002-6205-6566

Hatem Akbulut http://orcid.org/0000-0002-6299-136X
Serdar Aslan http://orcid.org/0000-0001-5061-6338

References

[1] Chen WY, Chen HW, Li WP, et al. Compositionally modulated microstructure in nano-layered Ni-P metallic glass composite coating prepared by electrodeposition. Surf Coat Technol. 2020;389:125636.
[2] Ünal E, Yaşar A, Karahan İH. A review of electrodeposited composite coatings with Ni-B alloy matrix. Mater Res Express. 2019;6:092004.
[3] Firouzi-Nerbin H, Nasirpouri F, Moslehifard E. Pulse electrodeposition and corrosion properties of nanocrystalline nickel-chromium alloy coatings on copper substrate. J Alloy Compd. 2020;822:153712.
[4] Zhang M, Zhu C, Yang C, et al. Preparation of amorphous Ni-W coating for the current collector of Na/S battery by electrodeposition. Surf Coat Technol. 2018;346:40–47.
[5] Torabinejad V, Aliofkhazraei M, Assareh S, et al. Electrodeposition of Ni-Fe alloys, composites, and nano coatings - A review. J Alloy Compd. 2017;691:841–859.
[6] Wasekara NP, Verulkar S, Vamsic MVN, et al. Influence of molybdenum on the mechanical properties, electrochemical corrosion and wear behavior of electrodeposited Ni-Mo alloy. Surf Coat Technol. 2019;370:298–310.
[7] Karimzadeh A, Aliofkhazraei M, Walsh FC. A review of electrodeposited Ni-Co alloy and composite coatings: microstructure, properties and applications. Surf Coat Technol. 2019;372:463–498.
[8] Mirak M, Akbari A. Microstructural characterization of electrodeposited and heat treated Ni-B coatings. Surf Coat Technol. 2018;349:442–451.
[9] Ogihara H, Udagawa K, Saji T. Effect of boron content and crystalline structure on hardness in electrodeposited Ni-B alloy films. Surf Coat Technol. 2012;206:2933–2940.
[10] Du Y, Zhang X, Wei L, et al. Electrodeposition of a Ni-P composite coating reinforced with $Ti_3C_2T_x$@TiO_2 /MoS_2 particles. Mater Chem Phys. 2020;241:122448.
[11] Li B, Zhang W, Huan Y, et al. Synthesis and characterization of Ni-B/Al_2O_3 nanocomposite coating by electrodeposition using trimethylamine borane as boron precursor. Surf Coat Technol. 2018;337:186–197.
[12] Gyawali G, Tripathi K, Joshi B, et al. Mechanical and tribological properties of Ni-W-TiB_2 composite coatings. J Alloy Compd. 2017;721:757–763.
[13] Li B, Zhang W, Zhang W, et al. Preparation of Ni-W/SiC nanocomposite coatings by electrochemical deposition. J Alloy Compd. 2017;702:38–50.
[14] Li B, Zhang W. Facile synthesis and electrochemical properties of a novel Ni-B/TiC composite coating via ultrasonic-assisted electrodeposition. Ultrason Sonochem. 2020;61:104837.
[15] Li D, Li B, Du S, et al. Synthesis of a novel Ni-B/YSZ metal-ceramic composite coating via single step electrodeposition at different current density. Ceram Int. 2019;45:24884–24893.
[16] Li B, Mei T, Li D, et al. Ultrasonic-assisted electrodeposition of Ni-Cu/TiN composite coating from sulphate-citrate bath: structural and electrochemical properties. Ultrason Sonochem. 2019;58:104680.
[17] Zhang W, Li B, Ji C. Synthesis and characterization of Ni-W/TiN nanocomposite coating with enhanced wear and corrosion resistance deposited by pulse electrodeposition. Ceram Int. 2019;45:14015–14028.
[18] Li B, Li D, Chen W, et al. Effect of current density and deposition time on microstructure and corrosion resistance of Ni-W/TiN nanocomposite coating. Ceram Int. 2019;45:4870–4879.
[19] Cui W, Zhang Y, Song R, et al. Ultrasonic assisted pulse electrodeposited Ni-doped TiN coatings. Ceram Int. 2018;44:14767–14773.
[20] Saha R, Khan T. Effect of applied current on the electrodeposited Ni-Al_2O_3 composite coatings. Surf Coat Technol. 2010;205:890–895.
[21] Deo Y, Guha S, Sarkar K, et al. Electrodeposited Ni-Cu alooay coatings on mild steel for enhanced corrosion properties. Appl Surf Sci. 2020;515:146078.
[22] Radwan AB, Ali K, Shakoor RA, et al. Properties enhancement of Ni-P electrodeposited coatings by the incorporation of nanoscale Y_2O_3 particles. Appl Surf Sci. 2018;457:956–967.
[23] Shakoor R, Kahraman R, Waware U, et al. Synthesis and properties of electrodeposited Ni-B-Zn ternary alloy coatings. Int J Electrochem Sci. 2014;9:5520–5536.
[24] Xu Y, Fan M, Luo Y, et al. Tribology and corrosion properties investigation of a pulse electrodeposition duplex hard-particle-reinforced Ni-Mo nanocomposite coating. Surf Coat Technol. 2020;393:125797.
[25] Beltowska-Lehman E, Indyka P, Bigos A, et al. Ni-W/ZrO_2 nanocomposites obtained by ultrasonic DC electrodeposition. Mater Des. 2015;80:1–11.
[26] Zhou Y, Xie FQ, Wu XQ, et al. A novel plating apparatus for electrodeposition of Ni-SiC composite coatings using circulating-solution co-deposition technique. J Alloy Compd. 2017;699:366–377.
[27] Guglielmi N. Kinetics of deposition of inert particles from electrolytic baths. J Electrochem Soc. 1972;119:1009–1012.
[28] Alizadeh M, Cheshmpish A. Electrodeposition of Ni-Mo/Al_2O_3 nano-composite coatings at various deposition current densities. Appl Surf Sci. 2019;466:433–440.
[29] Mehr MS, Akbari A, Damerchi E. Electrodeposited Ni-B/SiC micro- and nano-composite coatings: A comparative study. J Alloy Compd. 2019;782:477–487.
[30] Cerro Prada E, Torres Costa V, Herrero P, et al. Interface between cement paste and thin TiN film for corrosion resistance enhancement; structural, morphological and electrochemical properties. Constr Build Mater. 2015;80:48–55.
[31] Mirzamohammadi S, Khorsand H, Aliofkhazraei M, et al. Effect of carbamide concentration on electrodeposition and tribological properties of Al_2O_3 nanoparticle reinforced nickel nanocomposite coatings. Tribol Int. 2018;117:68–77.
[32] Masoudi M, Hashim M, Kamari HM. Characterization of novel Ni-Al_2O_3-SiC nanocomposite coatings synthesized by co-electrodeposition. Appl Nanosci. 2014;4:649–656.
[33] Pushpanathan DP, Alagumurthi N, Devaneyan SP. On the microstructure and tribological properties of pulse electrodeposited Ni-B_4C-TiC nano composite coating on AZ80 magnesium alloy. Surf Inter. 2020;19:100465.

[34] El-Sherik AM, Shirokoff J, Erb U. Stress measurements in nanocrystalline Ni electrodeposits. J Alloy Compd. 2005;389:140–143.
[35] Ranganatha S, Venkatesha TV, Vathsala K. Development of electroless Ni-Zn-P/nano-TiO_2 composite coatings and their properties. Appl Surf Sci. 2010;256:7377–7383.
[36] Skotnikova MA, Padgurskas J, Popov AA, et al. Localization of plastic deformation in HCP-, BCC-alloys and FCC-alloys at indentation. Mater Today. 2020;8. DOI:10.1016/j.matpr.2020.01.443.
[37] Zimmerman AF, Palumbo G, Aust KT, et al. Mechanical properties of nickel silicon carbide nanocomposites. Mater Sci Eng A. 2002;328:137–146.
[38] Tao Y, Ma F, Teng M, et al. Designed fabrication of super high hardness Ni-B-Sc nanocomposite coating for anti-wear application. Appl Surf Sci. 2019;492:426–434.
[39] Yan W, Pun CL, Simon GP. Conditions of applying Oliver-Pharr method to the nanoindentation of particles in composites. Compos Sci Technol. 2012;72:1147–1152.
[40] Hou KH, Chen YC. Preparation and wear resistance of pulse electrodeposited Ni-W/Al_2O_3 composite coatings. Appl Surf Sci. 2011;257:6340–6346.
[41] Wasekar NP, Bathini L, Ramakrishna L, et al. Pulsed electrodeposition, mechanical properties and wear mechanism in Ni-W/SiC nanocomposite coatings used for automotive applications. Appl Surf Sci. 2020;527:146896.
[42] Liu JH, Pei ZL, Shi WB, et al. Studies on preparation, microstructure, mechanical properties and corrosion resistance of Ni-Mo/micron-sized diamond composite coatings. Surf Coat Technol. 2020;385:125451.
[43] Hatipoglu G, Kartal M, Uysal M, et al. The effect of sliding speed on the wear behavior of pulse electro Co-deposited Ni/MWCNT nanocomposite coatings. Tribol Int. 2016;98:59–73.
[44] Bakhit B, Akbari A, Nasirpouri F, et al. Corrosion resistance of Ni-Co alloy and Ni-Co/SiC nanocomposite coatings electrodeposited by sediment co-deposition technique. Appl Surf Sci. 2014;307:351–359.
[45] Feng Q, Li T, Teng H, et al. Investigation on the corrosion and oxidation resistance of Ni-Al_2O_3 nano-composite coatings prepared by sediment co-deposition. Surf Coat Technol. 2008;202:4137–4144.
[46] Zhang R, Cui G, Su X, et al. A novel functionally graded Ni-graphene coating and its corrosion resistance. J Alloy Compd. 2020;829:154495.
[47] Reis FM, Melo HG, Costa I. EIS Investigation on Al 5052 alloy surface preparation for self-assembling monolayer. Electrochim Acta. 2006;51:1780–1788.
[48] Li B, Li D, Zhang J, et al. Electrodeposition of Ni-W/TiN-Y_2O_3 nanocrystalline coating and investigation of its surface properties and corrosion resistance. J Alloy Compd. 2019;787:952–962.
[49] Jiang W, Shen L, Qiu M, et al. Preparation of Ni-SiC composite coatings by magnetic field-enhanced jet electrodeposition. J Alloys Compd. 2018;762:115–124.